Figure S 1: Change in upward longwave radiative flux (W m^{-2}) per change of 0.1 in sea-ice concentration (slope of regression line) in the marine Arctic in February–March–April in four reanalyses (columns), based on the linear orthogonal-distance-regression (ODR) model. Dark grey indicates areas where the ODR model did not converge; in panels **(i)**−**(l)**, dark grey shows these areas in 1980–2000 and/or 2001–2021. Only grid cells with a mean of SIC > 0.5 were considered, and only the slopes whose 95 % confidence intervals do not overlap zero are shown (others masked in white). Points 1, 2, 3 (in yellow) from panels **(a), (c), (d)** are further analysed in Figure S2.
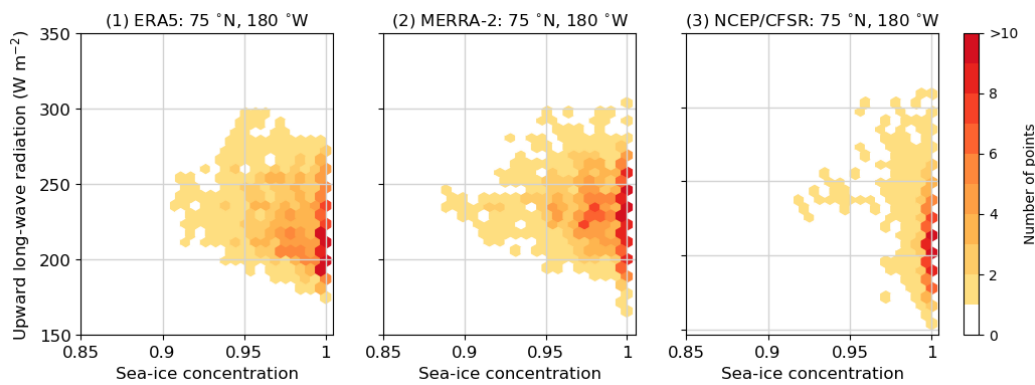
Figure S 2: Daily sea-ice concentration and upward long-wave radiative flux in selected grid cells on the border of Chukchi and East Siberian seas, where the orthogonal-distance-regression model did not converge. Data from ERA5 **(1)**, MERRA-2 **(2)**, and NCEP/CFSR **(3)** (as indicated in Figure S1 in panels **(a), (c), (d)**), grid cells nearest to 75° N, 180° E, days in February–March–April 1980–2000 (1875 days).
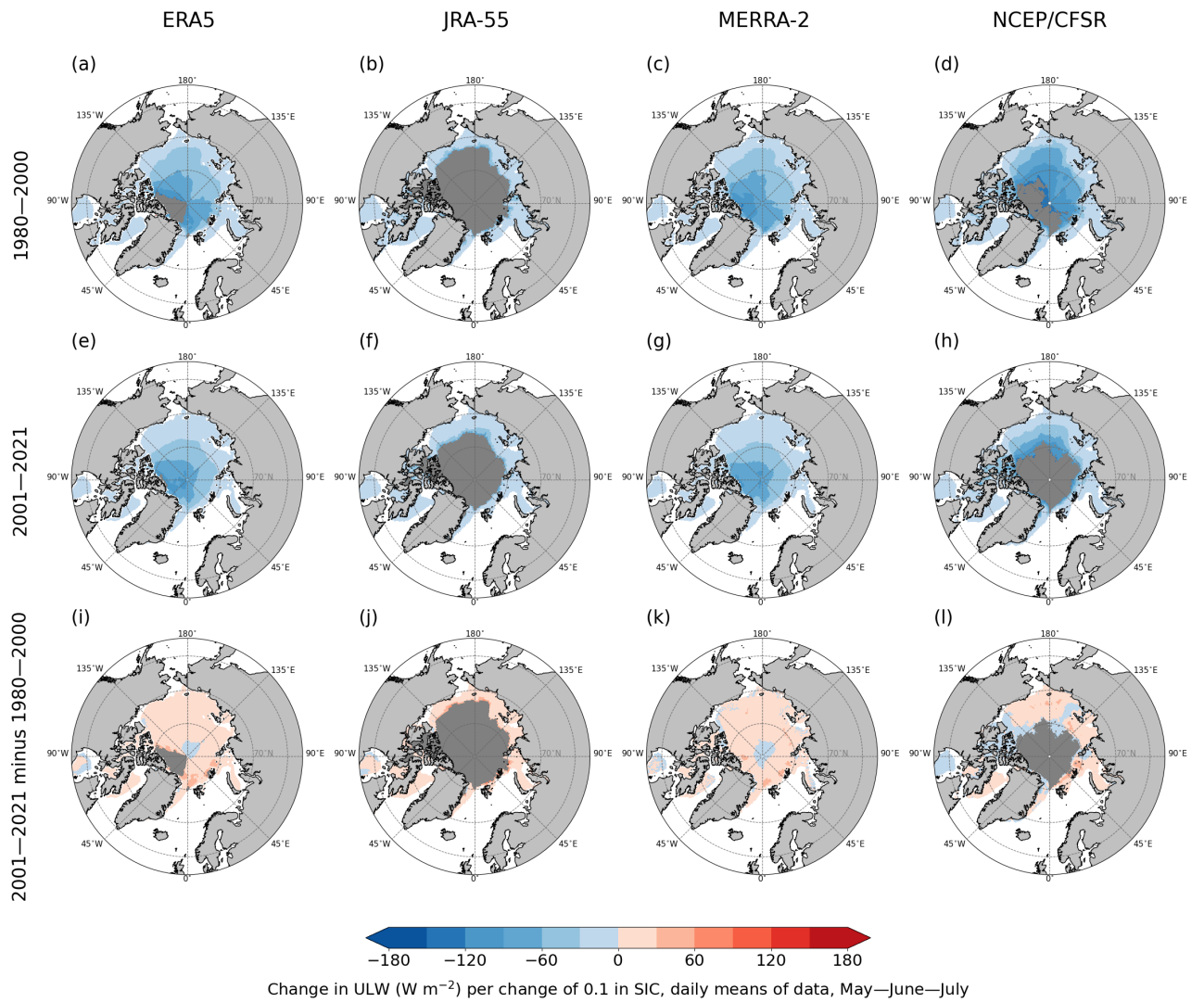
Figure S 3: Change in upward longwave radiative flux (W m^{-2}) per change of 0.1 in sea-ice concentration (slope of regression line) in the marine Arctic in May–June–July in four reanalyses (columns), based on the linear orthogonal-distance-regression (ODR) model. Dark grey indicates areas where the ODR model did not converge; in panels **(i)**−**(l)**, dark grey shows these areas in 1980–2000 and/or 2001–2021. Only grid cells with a mean of SIC > 0.5 were considered, and only the slopes whose 95 % confidence intervals do not overlap zero are shown (others masked in white).
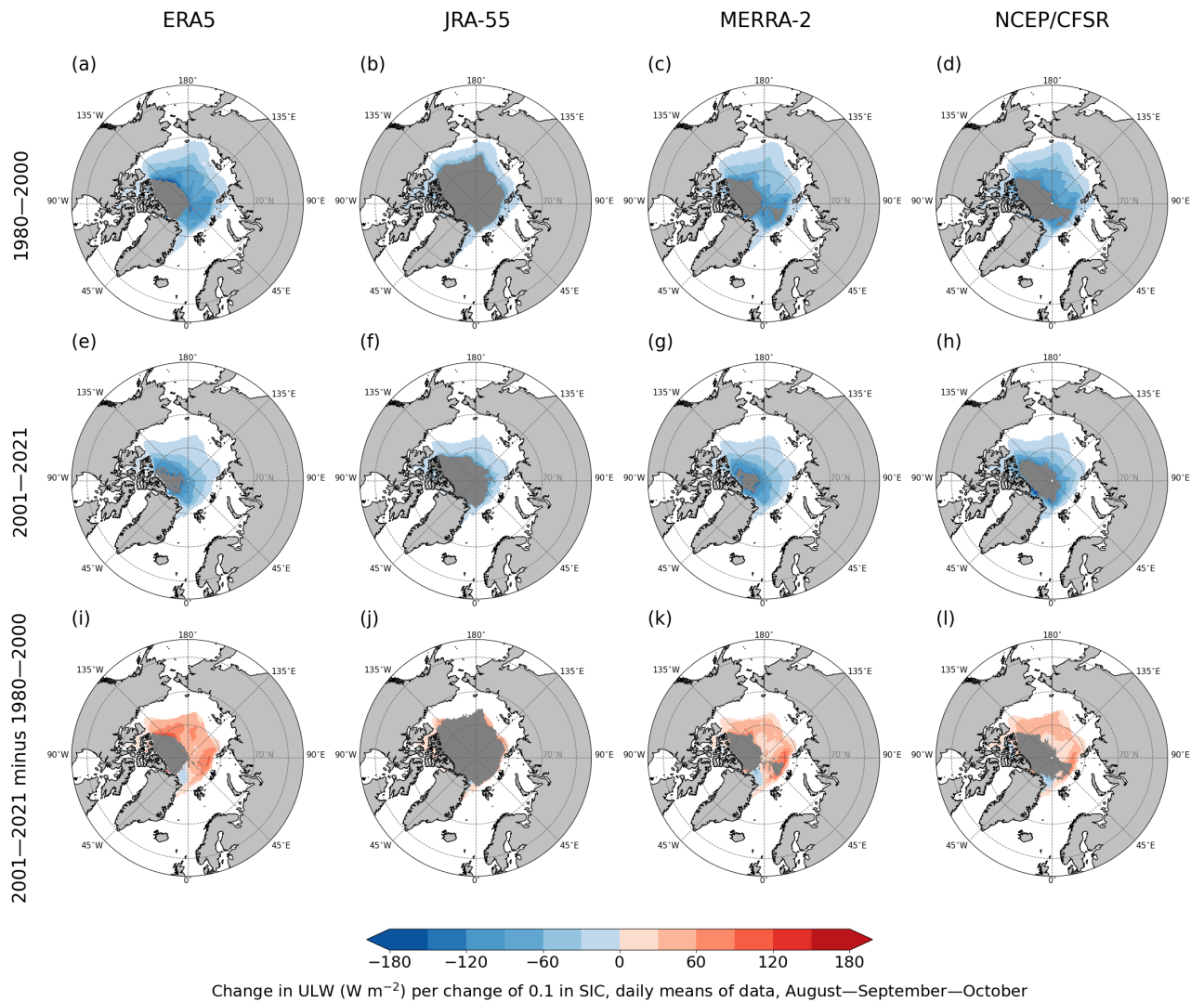
Figure S 4: Change in upward longwave radiative flux (W m^{-2}) per change of 0.1 in sea-ice concentration (slope of regression line) in the marine Arctic in August–September–October in four reanalyses (columns), based on the linear orthogonal-distance-regression (ODR) model. Dark grey indicates areas where the ODR model did not converge; in panels **(i)**–**(l)**, dark grey shows these areas in 1980–2000 and/or 2001–2021. Only grid cells with a mean of SIC > 0.5 were considered, and only the slopes whose 95 % confidence intervals do not overlap zero are shown (others masked in white).
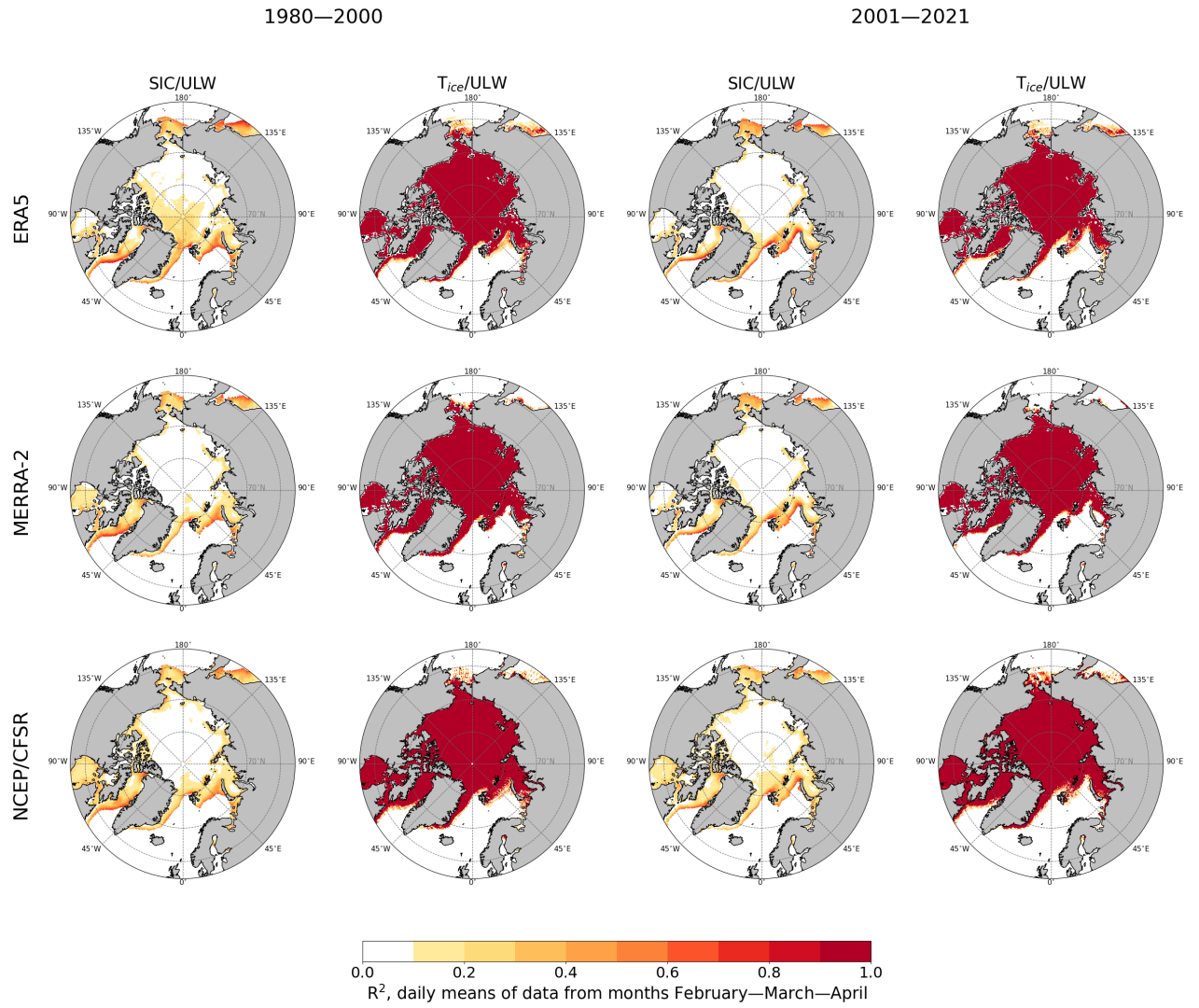
Figure S 5: Proportion of variance in the upward longwave radiation (ULW) explained by sea-ice concentration (SIC) and surface temperature of the ice (T_{ice}) in February–March–April, 1980–2000 and 2001–2021 (columns), as represented in three reanalyses (rows), based on linear ordinary-least-square regression model (coefficient of determination, R^2) using daily means of data from ERA5, MERRA-2, and NCEP/CFSR. Only grid cells with a mean of SIC > 0.5 were considered and only statistically significant results at the 5 % level of significance are shown (insignificant masked in white).
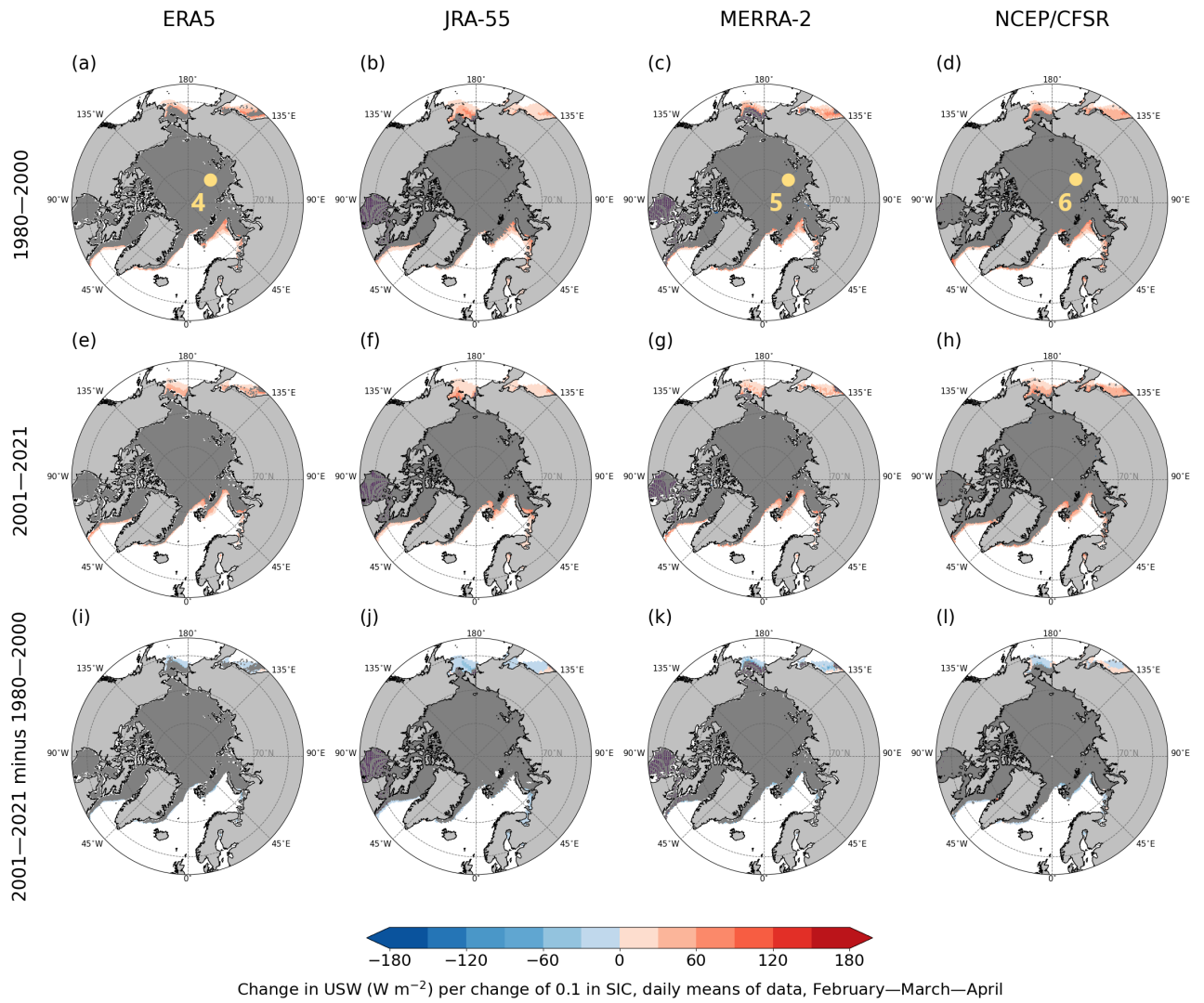
Figure S 6: Change in upward shortwave radiative flux (W m^{-2}) per 0.1 change in sea-ice concentration (slope of regression line) in four reanalyses (columns), marine Arctic, February–March–April, based on the linear orthogonal-distance-regression (ODR) model. Dark grey indicates areas where the ODR model did not converge; in panels **(i)**−**(l)**, dark grey shows these areas in 1980–2000 and/or 2001–2021. Only grid cells with a mean of SIC > 0.5 were considered, and only the slopes whose 95 % confidence intervals do not overlap zero are shown (others masked in white). Points 4, 5, 6 (in yellow) from panels **(a), (c), (d)** are further analysed in Figure S7.
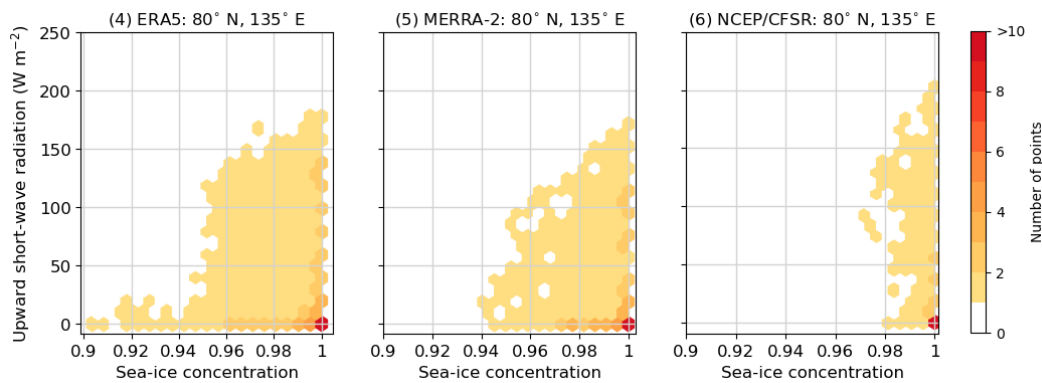
Figure S 7: Daily sea-ice concentration and upward shortwave radiative flux in selected grid cells in the Laptev Sea, where the orthogonal-distance-regression model did not converge. Data from ERA5 **(4)**, MERRA-2 **(5)**, and NCEP/CFSR **(6)** (as indicated in Figure S6 in panels **(a), (c), (d)**), grid cells nearest to 80° N, 135° E, days in February–March–April 1980–2000 (1875 days).

Change in USW (W m^{-2}) per change of 0.1 in SIC, daily means of data, August—September—October
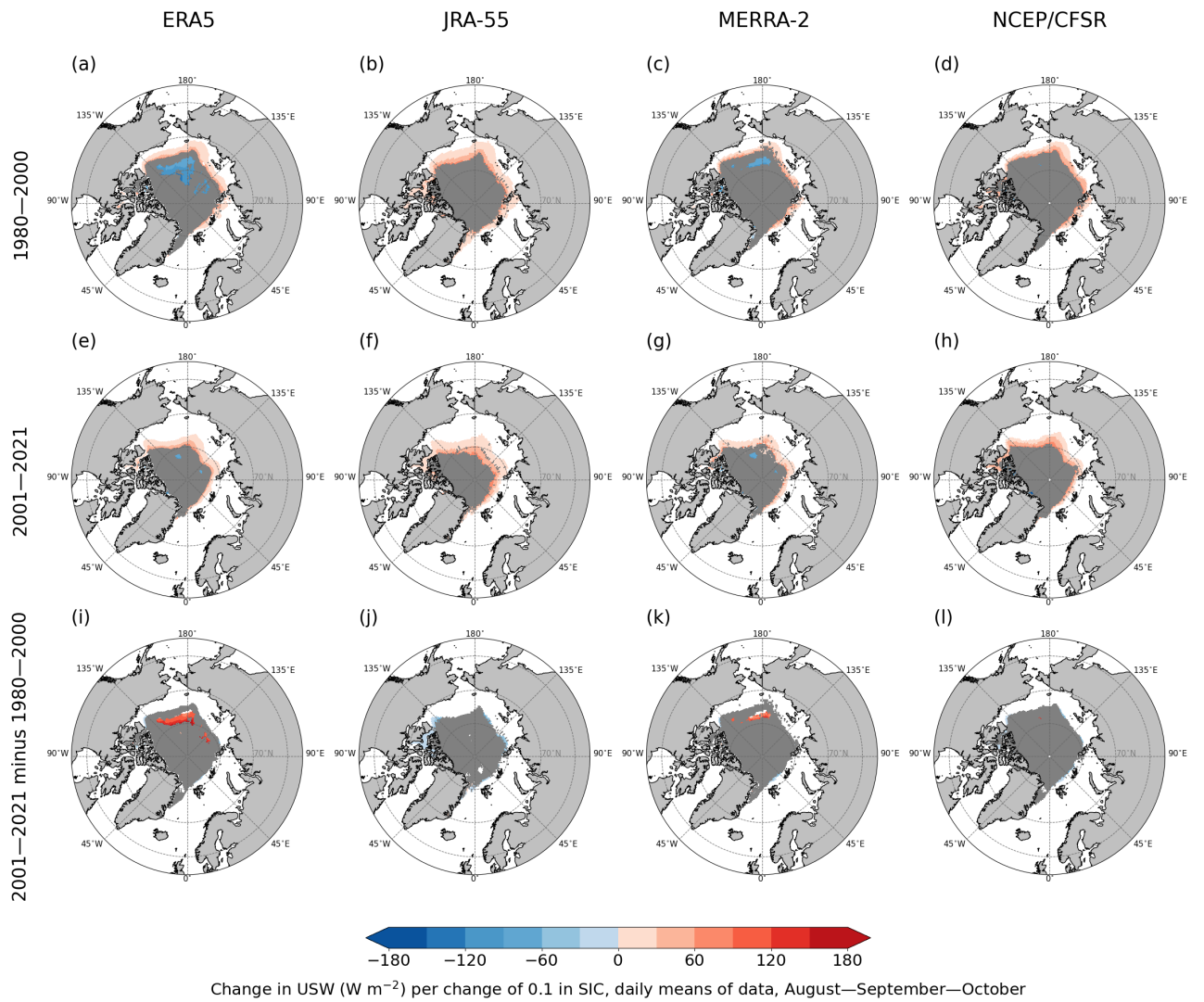
Figure S 8: Change in upward shortwave radiative flux (W m^{-2}) per 0.1 change in sea-ice concentration (slope of regression line) in four reanalyses (columns), marine Arctic, August–September–October, based on the linear orthogonal-distance-regression (ODR) model. Dark grey indicates areas where the ODR model did not converge; in panels **(i)−(l)**, dark grey shows these areas in 1980–2000 and/or 2001–2021. Only grid cells with a mean of SIC > 0.5 were considered, and only the slopes whose 95 % confidence intervals do not overlap zero are shown (others masked in white).
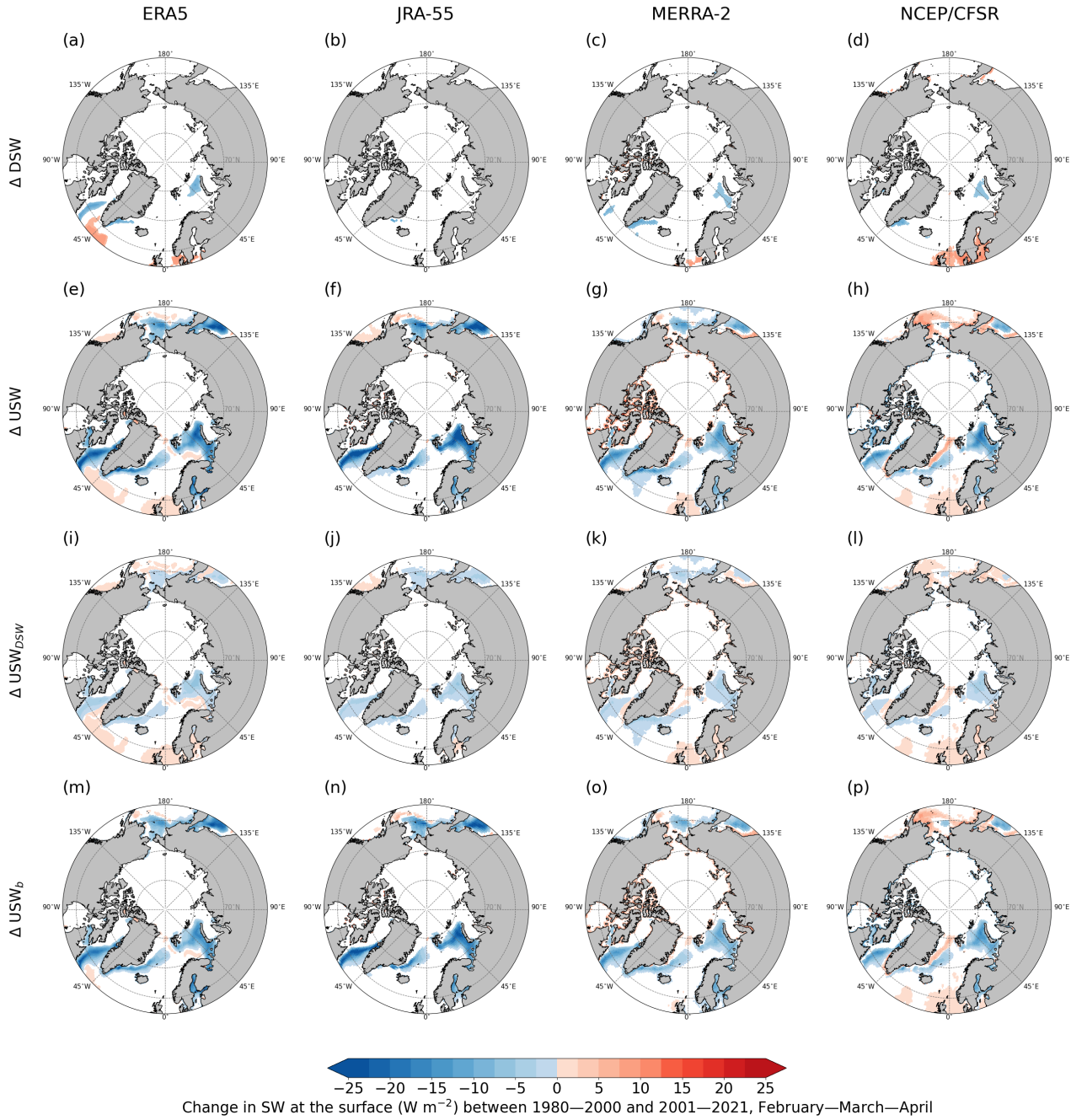
Figure S 9: Changes in decadal means (calculated from daily means) between 1980–2000 and 2001–2021, February–March–April. Panels **(a)–(h)** show changes in surface downward and upward shortwave radiative fluxes (ΔDSW, ΔUSW), panels **(i)–(l)** show changes in USW explained by changes in DSW (Δ USW$_{\mathrm{DSW}}$), and panels **(m)–(p)** changes in USW explained by changes in albedo (Δ USW$_{\mathrm{b}}$). Only statistically significant results at the 5 % level of significance are shown (insignificant masked in white); statistically significant grid cells for ΔUSW, Δ USW$_{\mathrm{DSW}}$, and Δ USW$_{\mathrm{DSW}}$ are identical. Values within an interval (-0.1,0.1) W m^{-2} are also masked in white.

Figure S 10: Changes in decadal means (calculated from daily means) 2001–2021 minus 1980–2000, February–March–April. Row **(i)** shows cloud condensate content (CCC, vertically integrated cloud liquid water + ice), row **(ii)** shows surface albedo, and row **(iii)** sea-ice concentration (SIC). Only statistically significant results at the 5 % level of significance are shown (insignificant masked in white). In rows **(ii)** and **(iii)**, values within an interval (-0.01,0.01) are also masked in white.
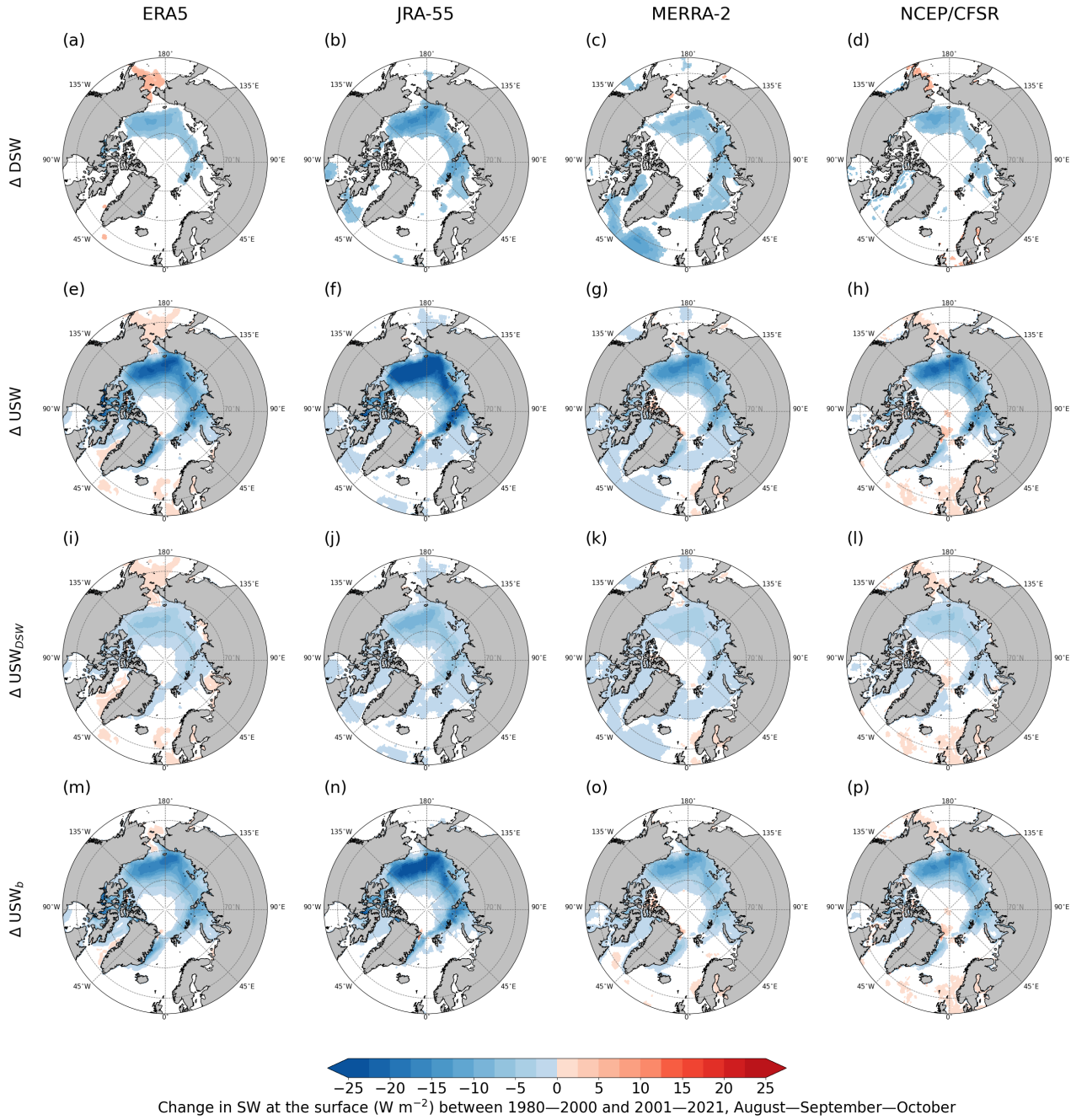
Figure S 11: Changes in decadal means (calculated from daily means) between 1980–2000 and 2001–2021, August–September–October. Panels **(a)−(h)** show changes in surface downward and upward shortwave radiative fluxes (ΔDSW, ΔUSW), panels **(i)−(l)** show changes in USW explained by changes in DSW ($\Delta\ \mathrm{USW_{DSW}}$), and panels **(m)−(p)** changes in USW explained by changes in albedo ($\Delta\ \mathrm{USW_b}$). Only statistically significant results at the 5 % level of significance are shown (insignificant masked in white); statistically significant grid cells for ΔUSW, $\Delta\ \mathrm{USW_{DSW}}$, and $\Delta\ \mathrm{USW_{DSW}}$ are identical. Values within an interval (-0.1,0.1) W m^{-2} are also masked in white.
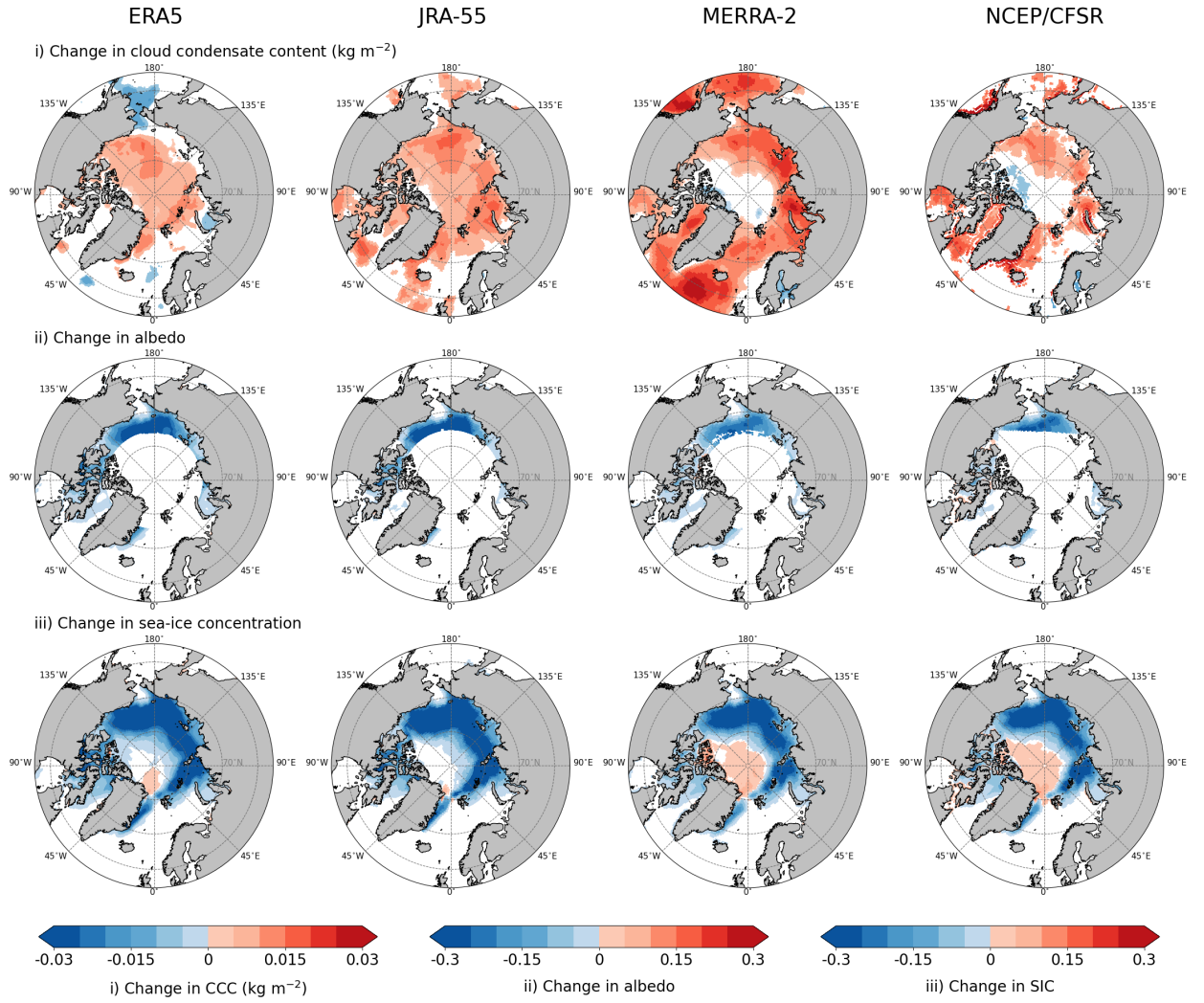
Figure S 12: Changes in decadal means (calculated from daily means) 2001–2021 minus 1980–2000, August–September–October. Row **(i)** shows cloud condensate content (CCC, vertically integrated cloud liquid water + ice), row **(ii)** shows surface albedo, and row **(iii)** sea-ice concentration (SIC). Only statistically significant results at the 5 % level of significance are shown (insignificant masked in white). In rows **(ii)** and **(iii)**, values within an interval (-0.01,0.01) are also masked in white.